
Explorable Decoding of Compressed Images

Yuval Bahat and Tomer Michaeli

Technion - Israel Institute of Technology, Haifa, Israel
{yuval.bahat@campus,tomer.m@ee}.technion.ac.il

Abstract

The ever-growing amounts of visual contents captured on a daily basis necessitate the use of lossy compression methods in order to save storage space and transmission bandwidth. While extensive research efforts are devoted to improving compression techniques, every method inevitably discards information. Especially at low bit rates, this information often corresponds to semantically meaningful visual cues, so that decompression involves significant ambiguity. In spite of this fact, existing decompression algorithms typically produce only a single output, and do not allow the viewer to explore the set of images that map to the given compressed code. Recently, explorable image restoration has been studied in the context of super-resolution. In this work, we propose to take this idea to the realm of image decompression. Specifically, we develop a novel deep-network based decoder architecture for the ubiquitous JPEG standard, which allows traversing the set of decompressed images that are consistent with the compressed input code. To allow for simple user interaction, we also develop a graphical user interface that comprises several intuitive exploration and editing tools. We exemplify our framework on graphical, medical and forensic use cases, demonstrating its wide range of potential applications.

1 Introduction

With surveillance systems so widely used and social networks ever more popular, the constant growth in the capacity of daily captured visual data necessitates using lossy compression algorithms (e.g. JPEG, H.264), that discard part of the recorded information in order to reduce storage space and transmission bandwidth. Over the years, extensive research has been devoted to improving compression techniques, whether by designing better decoders for existing encoders, or by devising new compression-decompression (CODEC) pairs that enable more loyal reconstruction at any given bit-rate. However, in any lossy compression method, the decoder faces inevitable ambiguity, which becomes particularly severe at low bit-rates. This is exemplified in Fig. 1 in the context of the JPEG compression standard. Low bit-rate compression may prevent the discrimination between a car's headlights and backlights, or the correct identification of a shirt pattern, a barcode, or text. Yet, despite this inherent ambiguity, existing decoders do not allow the user to explore the abundance of plausible images that could have been the source of a given compressed code.

Recently, there has been growing research focus on models that can produce diverse outputs for any given input, e.g. for image synthesis [6, 19, 38] and image reconstruction [16] tasks. In the context of super resolution, the works of [3, 4] took another step further, and allowed a user to traverse the space of high resolution images that correspond to a given low resolution input. In this paper, we propose to adapt this approach to the realm of visual decompression, and specifically illustrate *explorable image decompression* for the ubiquitous JPEG standard.

Our framework consists of a graphical user interface (GUI), allowing a user to interactively explore the space of perceptually pleasing decompressed images that could have given rise to the compressed input code (see Fig. 2). We utilize a novel image decompression network that predicts the quantization



Figure 1: **Ambiguity in JPEG decomposition.** A compressed JPEG file can correspond to numerous different plausibly looking images. These can vary in color, texture, and other structures that encode important semantic information. Since multiple images map to the same JPEG code, any decoder that outputs only a single reconstruction, fails to convey to the viewer the ambiguity regarding the encoded image.

errors of the DCT coefficients, and is thus guaranteed to produce outputs that are consistent with the compressed code. Unlike most methods, our design is oblivious to the JPEG *quality factor* (QF) parameter, which determines the average quantization interval size. This allows us to train a single model for all compression levels. A distinctive feature of our scheme is that it has a control input signal that can be used to manipulate the output. This, together with adversarial training, allows our decoder to generate diverse photo-realistic outputs for any given compressed input code.

Our approach is of wide applicability. Potential use cases range from allowing a user to restore lost information based on prior knowledge they may have about the captured image, through correcting unsatisfying decompression outputs (demonstrated in Fig. 7), to situations where a user wants to test specific hypotheses regarding the original image. The latter setting is particularly important in forensic image analysis and in medical image analysis, as exemplified in Fig. 3.

2 Related Work

Explorable image restoration The idea of explorable image restoration was presented in [3] and further studied in [4], but had not been applied to domains other than super-resolution to date. In the context of image compression, Guo and Chao [16] presented a method that can generate diverse outputs. However, it does not allow to systematically explore the set of consistent solutions, which is our goal in the current paper.

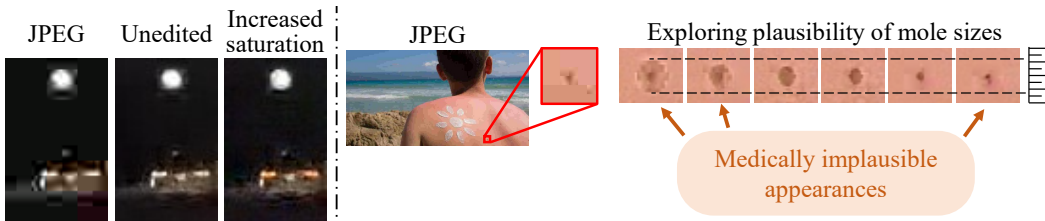
Compression techniques In recent years, a lot of research has been invested in devising new compression algorithms by learning them in an end-to-end manner, aiming to minimize reconstruction distortion (*e.g.* [1, 24]) or maximize perceptual quality (*e.g.* [2]), per bit-rate. Such methods show great potential in improving upon classical compression methods, but seem to have narrow applicability until integrated into some popular compression standard. An alternative line of work seeks to improve existing compression methods. This is done either by preprocessing the images prior to compressing them with a given encoder [8, 28] or by modifying the decompression pipeline for existing compression standards [5, 7, 7, 10, 18, 20–22, 27, 36, 39]. In principle, *explorable image decompression* can be considered within any of those frameworks. However, here we choose to demonstrate it for the latter category due to its wider practical applicability, where we specifically focus on the prevalent JPEG standard.

Improved JPEG decomposition Classical methods for JPEG artifact reduction (AR) [5, 20, 22] attempted different heuristics, like smoothing DCT coefficients [5] or relying on natural image priors like sparsity, in both DCT and pixel domains [22]. Deep convolutional AR networks (first proposed by Dong *et al.* [9]) learn to minimize a reconstruction error with respect to ground truth reference images, and operate either in the pixel [9, 32, 36, 39], DCT [31, 35] or both domains [15, 16, 18, 34, 37]. Some recent AR methods [11, 12, 17] use a generative adversarial network (GAN) scheme [13] for encouraging more photo-realistic results, which we too employ in our framework.

Consistent decoding Unlike our consistency ensuring design, outputs of existing methods (with the exception of [31]) are not guaranteed to be consistent with their corresponding compressed input



Figure 2: **Example exploration process.** Our GUI enables the user to explore the enforcement of various properties on any selected region within the image. Our method then seeks to conform to the user’s edits, while restricting the output to be (i) naturally looking, and (ii) perfectly consistent with the compressed code.



(a) Headlights or backlights?

(b) What size is the mole?

Figure 3: **Forensic and medical applications of our method.** (a) The car in this compressed surveillance footage (left and middle) seems to have white lights, which can be used to time an incident involving this *approaching* car. However, using our method reveals that the compressed image code also matches an alternative appearance of a *receding* car (right), inducing a completely different incident timing. (b) A dermatologist examining a suspected mole on a new patient may turn to existing patient photos containing this mole, to study its development. As the mole appearance in such images may often be degraded due to compression, our method can assist diagnosis by allowing exploration of the range of possible mole shapes and sizes. Please see corresponding editing processes in supplementary.

code. Kim *et al.* [17] tried to promote “faithful” outputs during training, by verifying their fidelity with respect to the corresponding ground truth images. In contrast, we avoid clinging to a specific reference solution, and instead allow producing any plausible output that would have been mapped to the given input code.

Quality factor Our design (as well as those in [18, 36, 39]) is oblivious to the QF parameter, and can therefore handle a wide range of compression levels. In contrast, other methods are trained for a fixed QF setting, which is problematic not only because it requires training a different model for each QF, but also since QF by itself is an ambiguous parameter, as its conversion into compression level varies across implementations.

3 Our Consistent Decoding Model

To enable exploration of our decompression model’s outputs, we need to verify they are both perceptually plausible and consistent with the given compressed code. To satisfy the first requirement, we adopt the common practice of utilizing an adversarial loss, which penalizes for deviations from the statistics of natural images. To satisfy the consistency requirement, we introduce a novel network design, that is specifically tailored for the JPEG compression format. The JPEG encoding scheme uses separate pipelines for the luminance (Y) and chrominance (Cb and Cr) channels of the image¹. Our model supports color images, however for the sake of clarity, we start by describing the simpler case of a gray-scale (single-channel) image. The non-trivial treatment of color is deferred to Sec. 4. We begin with a brief description of the relevant components in the JPEG compression pipeline, before describing our network design.

¹JPEG expects a $Y - Cb - Cr$ representation of input color images.

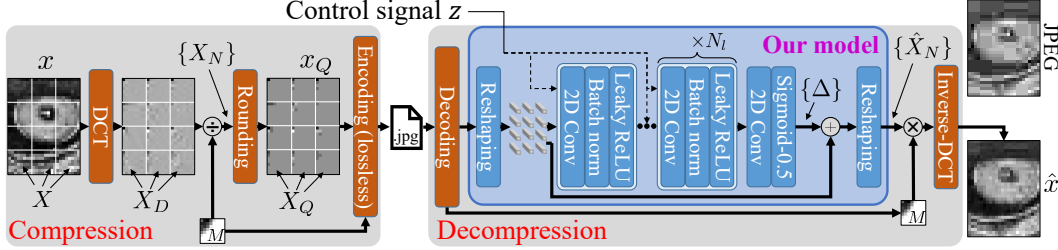


Figure 4: **JPEG compression scheme and our model.** Our network (inside the blue rectangle) is incorporated into the JPEG decompression pipeline in a way that guarantees the consistency of its outputs with the JPEG file content, while yielding a significant perceptual quality gain compared to images decompressed using the standard pipeline (top-right). An additional input signal z is incorporated to allow manipulating the output. Please refer to the description in Sec. 3.

3.1 JPEG compression

The encoding process is shown at the left hand side of Fig. 4. It starts by dividing the input image x , which is assumed to be of size² $8m \times 8n$, into an $m \times n$ array of non-overlapping 8×8 blocks. For each 8×8 block X , the encoder computes its DCT, $X_D = \text{DCT}(X)$, and divides it element-wise by a pre-defined matrix $M \in \mathbb{Z}^{8 \times 8}$ to obtain the block of normalized DCT coefficients $X_N = X_D \oslash M$. Finally, the entries of X_N are rounded to yield the block of quantized coefficients $X_Q = \text{round}(X_N)$. The blocks $\{X_Q\}$ are stored into the JPEG file alongside matrix M using some additional *lossless* processing steps. Note that the matrix M comprises the per-coefficient quantization intervals, determined as a function of the scalar QF parameter. However, this function varies between JPEG implementations, and therefore the QF itself is ambiguous and insufficient for extracting the image.

3.2 Our decoder design

Our decoder network is shown at the right hand side of Fig. 4. Our network operates in the DCT domain. Namely, for each 8×8 block X_Q extracted from the file, our network outputs an estimate \hat{X}_D of the corresponding block X_D . The decoded image is then constructed by applying inverse DCT on the predicted DCT blocks $\{\hat{X}_D\}$. To predict X_D , we first generate a prediction \hat{X}_N of the normalized coefficients X_N , and then multiply it element-wise by M , so that $\hat{X}_D = \hat{X}_N \odot M$. Since the only source of information loss is the rounding step, we consider a reconstructed block \hat{X}_N to be consistent with the quantized block X_Q when it satisfies $\hat{X}_N = X_Q + \Delta$, with an 8×8 matrix Δ whose entries are all in $[-0.5, 0.5)$. We therefore design our network to predict this Δ for each block, and we confine its entries to the valid range using a shifted Sigmoid function. The predicted residual Δ is then added to X_Q to form \hat{X}_N . This process guarantees that the decoded image is perfectly consistent with the compressed input code.

Predicting the residual Δ for each block X_Q is done as follows. We arrange the blocks $\{X_Q\}$ to occupy the channel dimension of an $m \times n \times 64$ tensor x_Q , so that each block retains its relative spatial position w.r.t. the other blocks in the image. We then input this tensor to a network comprising N_ℓ layers of the form 2-D convolution \rightarrow batch normalization \rightarrow leaky ReLU, followed by an additional 2-D convolution and a Sigmoid. The last convolution layer outputs 64 channels, which correspond to the residual blocks $\{\Delta\}$. Compared to operating in the pixel domain, the receptive field of this architecture is $8 \times$ larger in each axis, thus allowing it to exploit larger scale cues.

An important distinction of our network is the ability to manipulate its output, which facilitates our goal of performing explorable image decompression. This is enabled by incorporating a control input signal, which we feed to the network in addition to the quantized input x_Q . We define our control signal $z \in \mathbb{R}^{m \times n \times 64}$ to have the same dimensions as x_Q , so as to allow intricate editing abilities. Following the practice in [3], we concatenate z to the input of each of the N_ℓ layers of our network, to promote faster training.

²We focus on the case of integer m and n values for simplicity, but the compression process and our framework can be easily extended to handle images of all sizes.

We train our model following the general procedure of [3]. As an initialization step, we train it to minimize the L_1 distance between ground truth, uncompressed training images, and the corresponding outputs of our network, while randomly drawing the QF parameter for each image. Once initialized, training continues without utilizing any full-reference loss terms like L_1 or VGG, which is made possible thanks to the inherent consistency guarantee of our design. These full-reference loss terms are known to bias the output towards the (overly-smoothed) average of all possible explanations to the given compressed code, and are thus not optimal for the purpose of exploration. We instead minimize the following weighted combination of loss terms to guide our model:

$$\mathcal{L}_{\text{Adv}} + \lambda_{\text{Range}} \mathcal{L}_{\text{Range}} + \lambda_{\text{Map}} \mathcal{L}_{\text{Map}}. \quad (1)$$

Here, \mathcal{L}_{Adv} is an adversarial loss, which encourages the reconstructed coefficient blocks \hat{X}_D to follow the statistics of their natural image counterparts. In particular, we employ a Wasserstein GAN loss with spectral normalization [26] and gradient penalty [14], and use the same model architecture for both generator and critic (except for substituting batch normalization with layer normalization in the latter), following the recommendations in [14]. The second loss term, $\mathcal{L}_{\text{Range}}$, penalizes for pixel values in the resulting image \hat{x} that exceed the valid range $[0, 255]$, and thus helps prevent model divergence. We use $\mathcal{L}_{\text{Range}} = \frac{1}{k} \|\hat{x} - \text{clip}_{[0, 255]} \{\hat{x}\}\|_1$, where $k = 64 \cdot m \cdot n$ is the number of pixels in the image.

The last loss term in (1) is associated with the control signal z , which at exploration (test) time should allow traversing the space of plausible consistent decompressed images. Therefore, at train time, we want to encourage our network’s mapping of the space of control signals z onto the manifold of perceptually plausible images, that are consistent with input code x_Q . Denoting our network output by $\hat{x} = \psi(x_Q, z)$, we would like to guarantee that ψ can generate every plausible image \hat{x} with some choice of z . To this end, we introduce the loss term $\mathcal{L}_{\text{Map}} = \min_z \|\psi(x_Q, z) - x\|_1$, which penalizes for differences between the real natural image x , and its best possible approximation using some signal z . Within each training step, we first solve the internal minimization of \mathcal{L}_{Map} over z for 10 iterations, and then freeze this z for the minimization of all loss terms in (1).

3.3 Training details

We train our model on 1.15M images from the ImageNet training set [29], using batches of 16 with an Adam optimizer with learning rates of 0.0001 and 0.00001 for the initialization and consecutive training phases, respectively. To create training input codes, we compress the GT training images utilizing a quantization interval matrix $M = \text{QF} \cdot Q_{\text{baseline}}/5000$, where QF is independently sampled from a uniform distribution over $[5, 49]$ for each image³, and Q_{baseline} is the example baseline table in the JPEG standard [33]. We use $N_\ell = 10$ layers for both the generator and the critic models, using 320 output channels for all convolution operations but the last. We employ a conditional critic, which means we concatenate the generator’s input x_Q to our critic’s input, as we find it to accelerate training convergence.

4 Handling Color Channels

The JPEG standard works in the $Y - Cb - Cr$ color space. In this space, the color image x has three channels, which we denote by x^Y , x^{Cb} , and x^{Cr} . The chrominance channels (Cb and Cr) of natural images tend to contain mostly low frequency content. The JPEG format exploits this fact, by allowing to subsample those channels in the pixel space. The subsampled channels are then divided into 8×8 blocks, whose DCT coefficients are quantized, similarly to the luminance channel. This results in lost chroma information, which like its luminance counterpart, may correspond to semantically meaningful visual cues. Our framework allows exploring both the luminance and the chrominance of the image.

In this work, we use the most aggressive “4:2:0” subsampling configuration of JPEG, corresponding to subsampling the chroma channels by a factor of 2 in both axes. We reconstruct the chroma channels using an additional network, which handles the chroma information loss due to quantization. While we can use the same process employed in the luminance case to handle the chroma quantization,

³We omit the upper QF range of $[50, 100]$ when demonstrating our approach, as these higher QF values induce lower data loss, leaving less room for exploration.

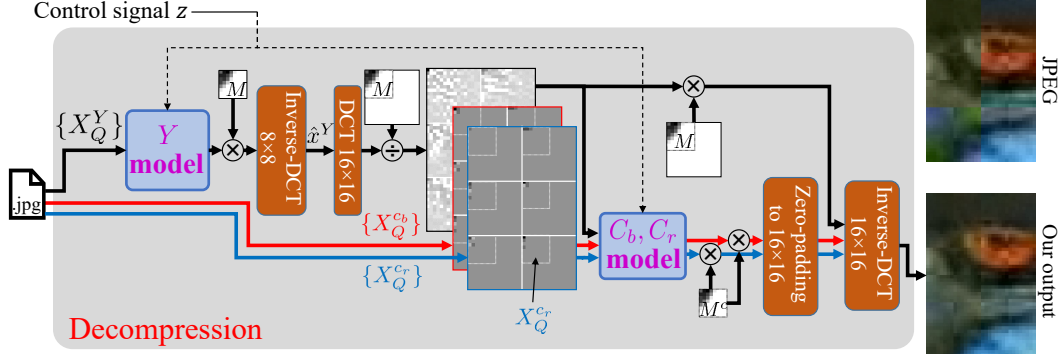


Figure 5: **Our full image decompression scheme.** We employ separate models (blue rectangles) to compensate for the luminance and chroma channels quantization errors. Both models share the same internal design depicted in Fig. 4, and receive the same control signal z , to allow coordinated editing. Please refer to the full description in Sec. 4.

accounting for subsampling requires some modifications. We begin by briefly describing the relevant steps in the JPEG chroma pipeline, and then elaborate on the modifications to our network design, both of which depicted in Fig. 5.

4.1 JPEG chroma subsampling

In order to produce high quality color outputs, we would like our chroma reconstruction network to be aware of the corresponding luminance information, ideally by concatenating it to the network’s compressed chroma input. However, this is impractical, as compressing with the “4:2:0” configuration involves computing DCT coefficients for each 8×8 block *after* subsampling each chroma channel, resulting in spatial dimensions’ inconsistency with the luminance channel. To overcome this hurdle, we remodel the above described subsampling pipeline using an approximated pipeline as follows.

Alternative modeling of the chroma subsampling process Since the contents of chroma channels of natural images are concentrated at the low frequencies, we assume that the quantized DCT coefficients of the subsampled chroma channels were obtained by rather computing the DCT of each 16×16 block of the original chroma channels, and extracting from it only the 8×8 block of coefficients corresponding to the low-frequency content. The rest of the process is modeled as is, resulting in 8×8 blocks of DCT coefficients quantized using matrix M^c . These blocks, denoted by $\{X_Q^{Cb}\}$ and $\{X_Q^{Cr}\}$, are stored in the color JPEG file alongside their luminance channel counterparts $\{X_Q^Y\}$. As we show in the Supplementary, the differences between images processed using the actual and approximated pipelines are negligible (*e.g.* PSNR = 88.9dB over the BSD-100 dataset [23]).

4.2 Modifying our design to support subsampling

Given a compressed input code, our framework first reconstructs the luminance channel, as described in Sec. 3. The reconstructed luminance image \hat{x}^Y is then fed into an additional network together with the quantized chroma blocks from the JPEG file, to obtain the final decoded color image.

Since the quantized 8×8 blocks of the chroma channels in fact correspond to 16×16 blocks of the image, our network operates on 16×16 blocks. Specifically, for the luminance channel \hat{x}^Y , we compute DCT coefficients for each 16×16 block and reshape them into a tensor with $16^2 = 256$ channels. The 8×8 chroma blocks stored in the file are zero-padded to be 16×16 in size (so that the high frequencies are all zeros) and then also reshaped into tensors with 256 channels (see Fig. 5). The luminance tensor is concatenated with the chrominance tensors to form a single tensor with $3 \times 256 = 768$ channels⁴. This tensor is then fed into our chroma network, which uses the same architecture described in Sec. 3, only with 160 channels in the internal layers. This network yields error estimate blocks Δ of size 8×8 , which are added to the quantized blocks X_Q^{Cb} and X_Q^{Cr} , and multiplied by M^c . The resulting blocks are zero-padded to 16×16 (setting the high frequencies to

⁴In practice, we discard the channels corresponding to the zero-padding, which are all zeros.

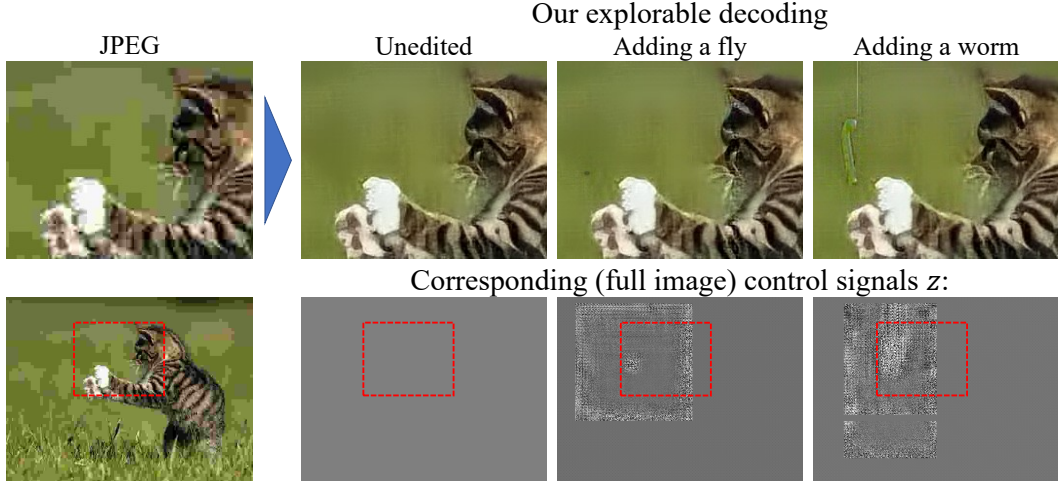


Figure 6: **Exploring plausible explanations.** Artifacts in the given compressed image (left) are removed by our method (middle-left) prior to any editing. We can then use our exploration GUI to produce different explanations to the kitten’s attention, by imprinting, *e.g.*, a tiny fly or a worm onto the unedited image. The resulting outputs (middle-right and right, respectively) are obtained through finding control signals z that correspond to the images best satisfying the imprinted content, while remaining consistent with the compressed image. The actual signals z corresponding to our three image versions are depicted in the bottom row, by converting their shape and range from $m \times n \times 64$ and $[-1, 1]$ to $8m \times 8n$ and $[0, 255]$, respectively.

zero) and converted back to pixel-space using inverse DCT. These reconstructed chroma channels are then combined with the luminance channel to yield the reconstructed color image. We feed the same control input signal z to both luminance and chroma models, to allow a coordinated editing effect.

5 Exploration Tools and Use Cases

Having trained both luminance and chroma models, we facilitate user exploration by employing a *graphical user interface* (GUI) comprising different editing tools. Our GUI runs on an NVIDIA GeForce 2080 GPU, and allows interactive exploration in real time. Specifically, once a compressed image code x_Q is loaded from a JPEG file, a user can manipulate the output of our decoding network, $\hat{x} = \psi(x_Q, z)$, by first marking a region to be edited and then choosing among different available tools. Those enable the user to attempt enforcing various properties on \hat{x} . Each editing tool triggers a process of solving $z^* = \arg \min_z f(\psi(x_Q, z))$ behind the scenes, for some objective function f , which is optimized using the Adam optimizer. The result is a modified output image $\psi(x_Q, z^*)$, which is guaranteed to be consistent with the compressed code x_Q (due to our network’s architecture) and to have a natural appearance (due to the parameters of ϕ which have been shaped at train time to favor natural outputs). Examples for such images \hat{x} and their corresponding signals z^* are depicted in Fig. 6.

We adapt most objective functions from [3] and modify them for the JPEG decompression case, while adding JPEG-specific objectives to allow tuning local hue and saturation. The full set of available objective functions facilitates a wide range of operations, including manipulating local image variance (*e.g.* using $f(\cdot) = (\text{Var}(\cdot) - c)^2$ for some desired variance level c), performing piece-wise smoothing (*e.g.* using $f(\cdot) = \text{TV}(\cdot)$), propagating patches from source to target regions, modifying periodic patterns and more.

A particularly useful group of tools allows embedding many forms of graphical user input, including various scribbling tools (similar to Microsoft-Paint), modifying local image brightness and even imprinting visual content from an external image. These tools act in two phases (corresponding to the middle pair of images in Fig. 2). In the first stage, they enforce consistency of the desired input with the compressed image code. This is done by projecting the scribbled (or imprinted) image onto the set of images that are consistent with the compressed code x_Q . Namely, each block of DCT



Figure 7: **Correcting unpleasing decompression.** Existing artifact removal methods like DnCNN [36] (middle-left), are often able to ameliorate compressed images (left), but do not allow editing their output. In contrast, outputs by our method (middle-right) can be edited by a user to yield superior results (right), which are guaranteed to be consistent with the compressed input code.



Figure 8: **Which war is over?** Using our framework to attempt imprinting years “1918” vs. “1945” yields a significantly better result for the former, suggesting this compressed archived newspaper dates back to the end of world war I.

coefficients $X_D^{\text{scribbled}}$ of the scribbled image is modified into

$$X_D^{\text{scribbled}} \leftarrow \left(\text{clip}_{[-\frac{1}{2}, \frac{1}{2}]} \left(X_D^{\text{scribbled}} \odot M - X_Q \right) + X_Q \right) \odot M. \quad (2)$$

This is the left of the middle pair in Fig. 2. In the second phase, an optimization process over z traverses the learned natural image manifold, searching for the output image that is closest to the consistent scribbled input. This is the right of the middle pair in Fig. 2. Variants of these tools provide many other features, including automatically searching for the most suitable embedding location, from a consistency standpoint. Please refer to the supplementary material for detailed descriptions of this and all other tools provided by our GUI.

Our exploration framework is applicable in many domains and use cases, which we demonstrate through a series of representative examples⁵. Fig. 7 depicts a visually unsatisfying decoded JPEG image (left). Utilizing an artifact removal method yields some improvement, but significant improvement is achieved by allowing a user to edit the image, harnessing specific prior knowledge about the appearance of sand dunes. Another important application involves exploring the range of plausible explanations to the compressed image code, like the different appearances of the shirt in Fig. 1 or the focus of the kitten’s attention in Fig. 6. Our framework can also be used to investigate which details could have comprised the original image. This is particularly important in medical and forensic settings. We demonstrate examples of exploring corrupted text in Fig. 8, and for investigating a suspected car from surveillance camera footage and examining a mole in a medical use case in Fig. 3.

6 Conclusion

We presented a method for user-interactive JPEG decoding, which allows exploring the set of naturally looking images that could have been the source of a compressed JPEG file. Our method makes use of a deep network architecture, which guarantees consistency with the compressed code by design. This network operates in the DCT domain, and has a control input signal that allows traversing the set of natural images that are consistent with compressed code. We demonstrated our approach in various use cases, showing its wide applicability in creativity, forensic, and medical settings.

⁵Compressed images in our examples are produced by applying the JPEG compression pipeline to uncompressed images, though our method is designed to allow exploration of existing compressed codes.

Broader Impact

Despite progress in compression algorithms, JPEG is still the most widely used image format, with billions of JPEG images produced on a daily basis. From photo albums to important sports or political events, JPEG images document the personal and collective experiences of many. Unfortunately, JPEG photos are not completely loyal to the scene they capture, as small and faint details are often lost in the compression process. When looking at such JPEG images (decompressed with a regular JPEG decoder), it is easy to tell that the quality in a certain region is not good enough. However, it is currently extremely difficult, if not impossible, to understand *what could and what could not have been there* in the original scene. Our method is the first to grant users the possibility of doing that.

We believe that our explorable decoding framework has the potential to see widespread use. One could envision integrating it into photo viewers and web browsers, from smartphones to desktop computers, as well as exploiting it in medicine and forensics.

A natural concern is the potential misuse of such technology. Visual contents could be edited to depict a misleading picture. However, it is important to stress that as opposed to existing editing software, our approach only allows making edits that are consistent with the JPEG file. This places a stringent constraint on the possible outputs that one could generate.

Appendices

A Exploration Tools

Our framework’s GUI comprises many editing and exploration tools that facilitate intricate editing operations. As we explain in Sec. 5, these tools work by triggering an optimization process over the space of control signals z , optimizing one of several possible objective functions $f(\cdot)$. This is analogous to traversing the manifold of perceptually plausible images learned by our network, while always remaining consistent with the compressed image code. Our GUI includes most of the editing tools introduced in the recent explorable super resolution work [3], by adapting the tools and corresponding objective functions for the JPEG decompression case. Editing can be applied to the entire image, or to a specific region marked by the user. Some tools enable more precise editing, by employing Microsoft-Paint-like buttons, including pen and straight line (with adjustable line width), as well as polygon, square and circle drawing tools.

We denote an output image prior to minimizing each objective f by $\hat{x}_0 = \psi(x_Q, z_0)$, where signal z_0 is either a neutral (pre-editing) control signal or the result of a prior editing process. Note that any function $f(\cdot)$ computed on the entire image can alternatively be computed on a specific region thereof, by masking out the rest of the image. We use $P(\cdot)$ to denote a patch extraction operator⁶, for those objective functions below that expect this kind of input. We next describe the different available objective functions and the way they are utilized in our GUI.

A.1 Variance Manipulation

This is a set of tools which operates by manipulating the local variance of all partially overlapping image patches in the selected region. We employ cost function $f(\hat{x}) = (\text{Var}(P(\hat{x})) - \text{Var}(P(\hat{x}_0)) - \delta)^2$, and optimize over z to modify (increase or decrease) the local, per-patch variance by a desired value δ .

A.2 Encouraging Piece-wise Smoothness

This tool acts by minimizing the total variations (TV) in an image or a region: $f(\hat{x}) = \text{TV}(\hat{x})$. In particular, we minimize the sum of absolute differences between each pixel in the image and its 8 neighboring pixels. This function can be minimized for a single region, or simultaneously minimized for several marked image areas.

⁶Objective functions operating on image patches (rather than directly on the image itself) use partially overlapping 6×6 patches. The degree of overlap varies, and indicated separately for each tool.

A.3 Imposing Graphical User Input

Our GUI comprises a large set of tools to allow imposing a graphical user input on the output image, by minimizing $f(\hat{x}) = \|\hat{x} - x^{\text{scribbled}}\|_1$. The desired graphical content $x^{\text{scribbled}}$ is imposed in a consistency preserving manner, by projecting it onto the set of images that are consistent with the compressed code x_Q . Namely, each block of DCT coefficients $X_D^{\text{scribbled}}$ of the desired input is modified by applying Eq. (2), repeated here for fluency:

$$X_D^{\text{scribbled}} \leftarrow \left(\text{clip}_{[-\frac{1}{2}, \frac{1}{2}]} \left(X_D^{\text{scribbled}} \odot M - X_Q \right) + X_Q \right) \odot M. \quad (3)$$

The modified $X^{\text{scribbled}}$ (depicted, *e.g.*, in the left of the middle pair of images in Fig. 2) is already consistent with the compressed input code x_Q . The user then has the option of translating, resizing or rotating the inserted content using arrow buttons, while consistency is re-enforced automatically after each of these operations. Editing is completed when the user initiates the optimization process, traversing the z space looking for the image \hat{x} that is closest to the desired consistent content $X^{\text{scribbled}}$, while lying on the learned manifold of perceptually plausible images.

The desired input $x^{\text{scribbled}}$ can originate from any of the following sources:

1. *User scribble*: A user can use the Microsoft-Paint-like drawing tools, where scribbling color can be chosen manually or sampled from any given image (including the edited one). Please see Fig. 9(b) for an example usage of this tool.
2. *Manipulating HSV*: Local hue, saturation and relative brightness (value) of \hat{x} can be manipulated by using one of 6 designated buttons. This results in a desired appearance $x^{\text{scribbled}}$, whose consistency is continuously enforced after each button press, by computing (2). Brightness manipulation was already facilitated in [3] for small image details, but larger regions could not be manipulated, as their HSV attributes are strictly determined by the low-resolution input. In contrast, JPEG compression often discards information corresponding to these attributes, thus allowing and necessitating their exploration. Please see Fig. 9(a) for an example usage of this tool.
3. *Imprinting*: A user can import graphical content, either from within the edited image or from an external one, and then enforce it on \hat{x} . The user first selects the desired content to import, and then marks the target region’s bounding rectangle on \hat{x} . JPEG compression operates on 8×8 pixel blocks, making it highly sensitive to small image shifts. Therefore, to adapt this tool from [3], we propose an option to automatically find a sub-block shifting of the imported content, that yields the most consistent imprinting. Please see Fig. 2 for an example usage of this tool.

Subtle region shifting A variant of the imprinting tool allows applying subtle local affine transformations. It works by imprinting the region of interest onto itself, then allowing a user to utilize the shifting, resizing and rotating buttons to modify the selected region from its original appearance, before triggering the final z optimization process.

A.4 Desired Dictionary of Patches

This tool manipulates target patches in a desired region to resemble the patches comprising a desired source region, either taken from an external image or from a different location in the edited image. The corresponding cost function penalizes for the distance between each patch in the target region and its nearest neighbor in the source region. To allow encouraging desired textures across regions with different colors, we first remove mean patch values from each patch, in both source and target patches. To reduce computational load, we discard some of the overlapping patches, by using 2 and 4 rows strides in the source and target regions, respectively. This tool was used for creating the result in Fig. 7 (right image), by propagating patches depicting sand-waves from the center of the image to its upper-left regions.

Ignoring patches’ variance A variant of this tool allows encouraging desired textures without changing current local variance. To this end, we normalize patches’ variance, in addition to removing their mean. Then while optimizing over z , we add an additional penalty that preserves the original variance of each target patch, while encouraging its (normalized) signal to resemble that of its closest (normalized) source patch.

A.5 Signal magnitude manipulation

An additional tool operating on image patches attempts to amplify or attenuate the magnitude of the signal in existing patches, while preserving existing patch structures. Similar to the variance manipulation tool described in Sec. A.1, we use $f(\hat{x}) = (\tilde{P}(\hat{x}) - (1 + \delta)\tilde{P}(\hat{x}_0))^2$ as our cost function. It penalizes for the difference between existing image patches and their $(1 + \delta)$ times magnified/attenuated counterparts, where operator $\tilde{P}(\cdot)$ extracts image patches and subtracts their respective mean values. This tool was also utilized for creating the result in Fig. 7 (right image), by enhancing the sand-wave appearance of patches propagated to the upper left image regions.

A.6 Encouraging Periodicity

This tool encourages the periodic nature of an image region, across one or two directions determined by a user. The desired period length (in pixels) for each direction can be manually set by the user, or it can be automatically set to the most prominent period length, by calculating local image self-correlation. Periodicity is then encouraged by penalizing for the difference between the image region and its version translated by a single period length, for each desired direction. We used this tool too when creating Fig. 7 (right image), for encouraging the sand-waves to have an approximately constant period length (in the appropriate direction), thus yielding a more realistic appearance.

A.7 Random Diverse Alternatives

This tool allows exploring the image manifold in a random manner, producing N different outputs by maximizing the L_1 distance between, them in pixel space. These images (or sub-regions thereof) can then serve as a baseline for further editing and exploration.

Constraining distance to current image A variant of this tool adds the requirement that all N images should be close to the current \hat{x}_0 (in terms of L_1 distance in pixel space).

B Editing Processes and Additional Examples

We next exemplify the exploration and editing process, and illustrate the effect of the quality factor (QF) on the available degrees of freedom.

Figure 9(a) shows the editing process used in Fig. 3(a). Here, the color of the car’s lights in the unedited output, is nearly pure white. However, by increasing the saturation in that region, we manage to turn the lights into red. The resulting image is consistent with the JPEG code and therefore constitutes an equally plausible reconstruction of the captured scene.

Figure 9(b) shows the exploration process of Fig. 3(b). Here, we attempted to imprint brown disks of varying radii on the unedited image. The top row shows the results of the first stage of the imprinting process, which projects the image with the naively placed brown disk onto the set of images that are consistent with the JPEG code. The second row shows the results of the second stage of the imprinting process, which seeks a control signal z that causes the output of our decoding network to resemble the image produced in the first stage. In this example, the second stage is mostly responsible for smoothing some of the artifacts generated in the first stage.

Figure 10 illustrates the effect of the QF on the space of images that are consistent with a given JPEG code. As can be seen, when using extreme compression with a QF of 5, we can produce consistent reconstructions with a wide range of mole sizes, from a very large mole on the left, to an almost vanished mole on the right. However, as the QF increases, the set of consistent solutions becomes smaller, making it impossible to imprint very large or very small disks.

C Quantitative Performance Comparison

Our JPEG decoding framework is the first to facilitate exploration of the abundant plausible images corresponding to a given compressed JPEG code, and therefore cannot be compared to any existing method. Nonetheless, it produces high quality outputs even prior to applying any user editing. To evaluate the quality of pre-edited outputs and compare it with that of existing JPEG artifact removal

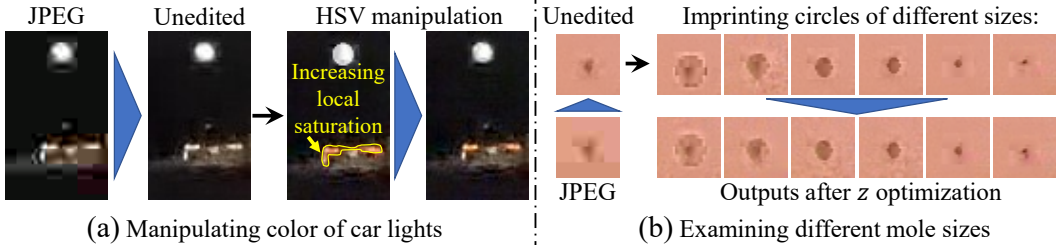


Figure 9: **The making of Fig. 3.** (a) The unedited output of our network decodes the car lights as nearly pure white. However, increasing the saturation in that region, reveals that red lights are an equally plausible explanation to the code stored in the JPEG file. (b) Here, we imprint brown disks of varying radii on the region of the mole. The top row shows the projection of the naively imprinted image onto the set of consistent solutions. The bottom row shows the final output of our method, after determining the control signal z that causes the net’s output to resemble the most to the images in the top row.

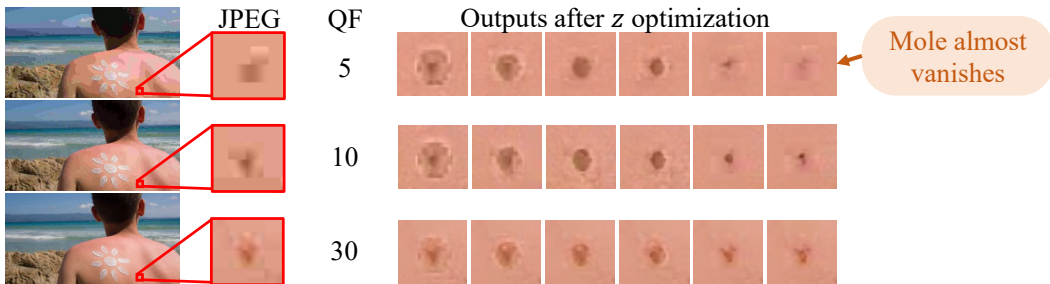


Figure 10: **Effect of QF on exploration space.** The ability to imprint brown disks of different radii on the mole, strongly depends on the QF. When the QF is small (aggressive compression), the space of consistent solutions is large. In this case, we can imprint a large mole in one extreme, or completely remove the mole in the other extreme. However, as the QF increases, the space of consistent solutions becomes smaller, and the range of mole sizes that can be imprinted reduces accordingly.

methods, we perform two experiments using two datasets commonly used for evaluating artifact removal, namely the LIVE1 [30] and BSD-100 [23] datasets.

Methods for removing JPEG artifact strive to achieve one of two possible goals; either they attempt to minimize outputs’ distortion (with respect to corresponding ground truth (GT) uncompressed images), or they try to maximize their outputs’ perceptual quality. We evaluate the performance with respect to each of these different goals, by adapting the commonly used metric for each goal: Distortion is evaluated by measuring peak signal to noise ratio (PSNR), while perceptual quality is evaluated using the naturalness image quality evaluator (NIQE) score [25], which is a no-reference image quality score.

Recall from Sec. 3 that training our model involves an initialization phase, in which the network is trained to minimize reconstruction error with respect to GT uncompressed images, and a consecutive phase, involving all loss terms in Eq. (1) and no full-reference loss terms. In this experiment, we evaluate both the model obtained at the end of initialization phase, trained to minimize distortion, and the final model, trained to maximize perceptual quality. We consider these two models as two different configurations, denoting them by “Ours (MSE)” and “Ours (GAN)”, respectively. We compare them with the results by the DnCNN method [36], which is the only existing artifact removal method that can be applied to a range of quality factors, like our method, and has its code available online. Since the available pretrained model of DnCNN can only handle single channel images (only the Y channel), we conduct our experiments using gray-scale images.

The evaluations of both metrics, on both datasets, are presented in Fig. 11. In all four evaluations, we include scores corresponding to the compressed JPEG images, and in the perceptual quality evaluation (bottom row) we also include scores for the GT images). The results indicate that our first model configuration (blue), trained to minimize distortion, performs better than DnCNN (brown) in terms of reconstruction error (top row), on both datasets, throughout the range of QFs. PSNR scores

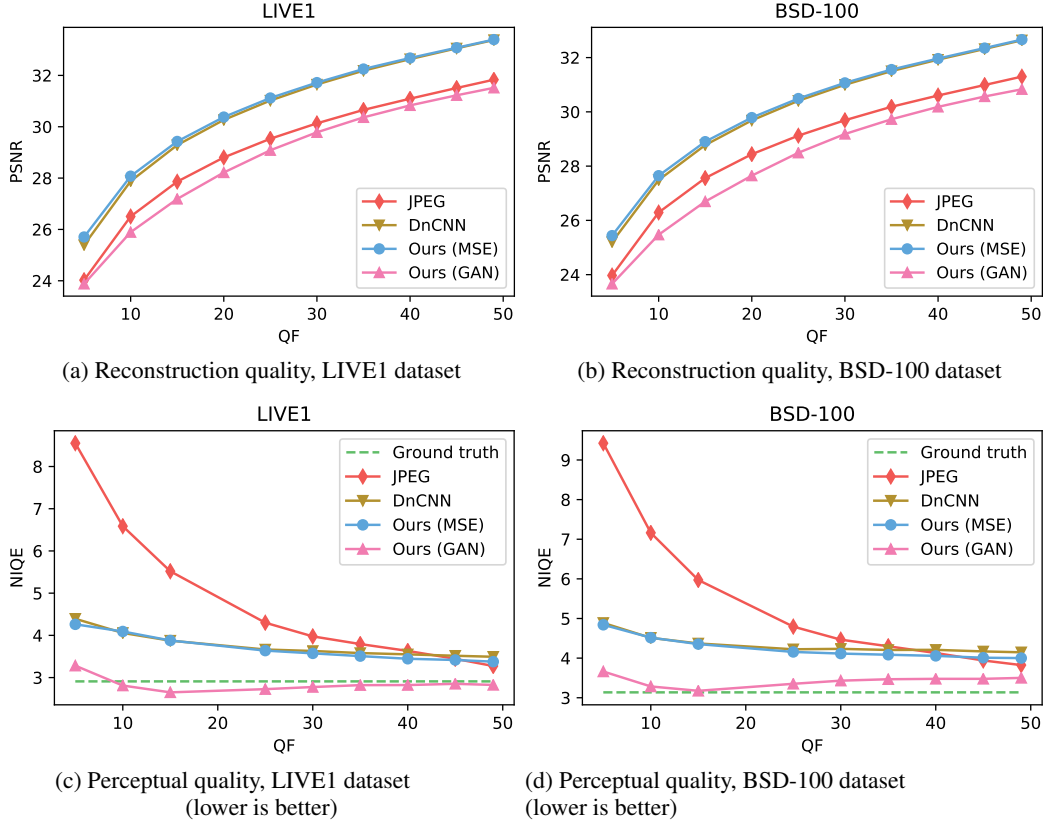


Figure 11: **Quantitative performance evaluation.** Comparing performance on the LIVE1 [30] (left column) and BSD-100 [23] (right column) datasets, in terms of image distortion (top row) or perceptual quality (bottom row), using the PSNR and NIQE metrics, respectively. Please see details in Sec. C.

of our 2nd configuration (pink), trained for perceptual quality, are significantly lower, surpassed even by the scores of the JPEG images.

As for perceptual quality (bottom row), NIQE scores (where lower is better) suggest that our GAN-trained model (pink) performs well across all evaluated QFs and both datasets, obtaining similar scores to those of the GT images. As expected, both our 1st model configuration and the DnCNN model perform significantly worse, as they were both trained to minimize distortion.

D Validating our Alternative Modeling of Chroma Subsampling

In an effort to produce higher quality reconstruction of the chroma information, we wish to concatenate the reconstructed luminance information \hat{x}^Y to the input of our chroma reconstruction model. However, this requires handling the dimensions inconsistency between the full-resolution luminance channel and the subsampled chroma channels, which we do through introducing an alternative modeling of the JPEG chroma subsampling process, as we explain in Sec. 4.1.

To validate this alternative modeling, we looked at the differences (calculated after going back to the pixel domain) between images undergoing the following original vs. alternative subsampling processes:

1. “4:2:0” JPEG pipeline: Subsampling chroma channels by a factor of 2 in both axes → Computing DCT coefficients for each 8×8 pixels block → Right and bottom zero-padding each coefficients block to 16×16 → Returning to pixel domain by computing inverse DCT for each 16×16 block.

2. *Our alternative pipeline:* Computing DCT coefficients for each 16×16 pixels block \rightarrow Setting each block’s 3 lower-right quadrants to 0, leaving unchanged the 8×8 upper left quadrant coefficients that correspond to low-frequency content \rightarrow Returning to pixel domain by computing inverse DCT for each 16×16 block.

Note that we did not perform any quantization step in either of the alternatives, as we were only interested in the isolated effect of remodeling the subsampling pipeline.

We computed the differences between the two alternatives using the RGB color representation, after concatenating back the non-altered luminance channel (Y) in both alternatives. We experimented using 100 images from the BSD-100 dataset [23], and found that the average root mean square error (RMSE) was a negligible 0.009137 gray levels (corresponding to a PSNR of 88.9dB). This certifies our decision to use the alternative modeling, which allows us to make our chroma reconstruction network aware of the corresponding luminance channel, by concatenating it to the network’s input.

E Full Training Details

We train our model on 1.15M images from the ImageNet training set [29], using batches of 16 images each. We use an Adam optimizer, with learning rates of 0.0001 and 0.00001 for the initialization and consecutive training phases, respectively, and set $\beta_1 = 0.9$ and $\beta_2 = 0.999$ for both generator and critic networks. After the initialization phase, we set λ_{Range} and λ_{Map} from Eq. (1) to 200 and 0.1 respectively, and perform 10 critic iterations for every generator iteration performed. To create compressed images input codes, we compress the GT training images utilizing a quantization interval matrix $M = \text{QF} \cdot Q_{\text{baseline}}/5000$, where QF is independently sampled from a uniform distribution over [5, 49] for each image⁷, and Q_{baseline} is the example baseline table in the JPEG standard [33]. We use $N_\ell = 10$ layers for both generator and critic models, where convolution operations utilize 3×3 spatial kernels with 320 or 160 output channels for all layers but the last, in the luminance or chroma networks, respectively. We employ a conditional critic, which means we concatenate the generator’s input x_Q to our critic’s input, as we find it to accelerate training convergence.

References

- [1] Eirikur Agustsson, Fabian Mentzer, Michael Tschannen, Lukas Cavigelli, Radu Timofte, Luca Benini, and Luc V Gool. Soft-to-hard vector quantization for end-to-end learning compressible representations. In *Advances in Neural Information Processing Systems*, pages 1141–1151, 2017.
- [2] Eirikur Agustsson, Michael Tschannen, Fabian Mentzer, Radu Timofte, and Luc Van Gool. Generative adversarial networks for extreme learned image compression. In *Proceedings of the IEEE International Conference on Computer Vision*, pages 221–231, 2019.
- [3] Yuval Bahat and Tomer Michaeli. Explorable super resolution. *arXiv preprint arXiv:1912.01839*, 2019.
- [4] Marcel Christoph Bühler, Andrés Romero, and Radu Timofte. Deepsee: Deep disentangled semantic explorative extreme super-resolution. *arXiv preprint arXiv:2004.04433*, 2020.
- [5] Tao Chen, Hong Ren Wu, and Bin Qiu. Adaptive postfiltering of transform coefficients for the reduction of blocking artifacts. *IEEE transactions on circuits and systems for video technology*, 11(5):594–602, 2001.
- [6] Wengling Chen and James Hays. Sketchygan: Towards diverse and realistic sketch to image synthesis. In *Proceedings of the IEEE Conference on Computer Vision and Pattern Recognition*, pages 9416–9425, 2018.
- [7] Yehuda Dar, Alfred M Bruckstein, Michael Elad, and Raja Giryes. Postprocessing of compressed images via sequential denoising. *IEEE Transactions on Image Processing*, 25(7):3044–3058, 2016.
- [8] Yehuda Dar, Michael Elad, and Alfred M Bruckstein. Optimized pre-compensating compression. *IEEE Transactions on Image Processing*, 27(10):4798–4809, 2018.
- [9] Chao Dong, Yubin Deng, Chen Change Loy, and Xiaoou Tang. Compression artifacts reduction by a deep convolutional network. In *Proceedings of the IEEE International Conference on Computer Vision*, pages 576–584, 2015.
- [10] Xueyang Fu, Zheng-Jun Zha, Feng Wu, Xinghao Ding, and John Paisley. Jpeg artifacts reduction via deep convolutional sparse coding. In *Proceedings of the IEEE International Conference on Computer Vision*, pages 2501–2510, 2019.
- [11] Leonardo Galteri, Lorenzo Seidenari, Marco Bertini, and Alberto Del Bimbo. Deep generative adversarial compression artifact removal. In *Proceedings of the IEEE International Conference on Computer Vision*, pages 4826–4835, 2017.

⁷We omit the upper QF range of [50, 100] when demonstrating our approach, as these higher QF values induce lower data loss, leaving less room for exploration.

- [12] Leonardo Galteri, Lorenzo Seidenari, Marco Bertini, and Alberto Del Bimbo. Deep universal generative adversarial compression artifact removal. *IEEE Transactions on Multimedia*, 21(8):2131–2145, 2019.
- [13] Ian Goodfellow, Jean Pouget-Abadie, Mehdi Mirza, Bing Xu, David Warde-Farley, Sherjil Ozair, Aaron Courville, and Yoshua Bengio. Generative adversarial nets. In *Advances in neural information processing systems*, pages 2672–2680, 2014.
- [14] Ishaan Gulrajani, Faruk Ahmed, Martin Arjovsky, Vincent Dumoulin, and Aaron C Courville. Improved training of wasserstein gans. In *Advances in neural information processing systems*, pages 5767–5777, 2017.
- [15] Jun Guo and Hongyang Chao. Building dual-domain representations for compression artifacts reduction. In *European Conference on Computer Vision*, pages 628–644. Springer, 2016.
- [16] Jun Guo and Hongyang Chao. One-to-many network for visually pleasing compression artifacts reduction. In *Proceedings of the IEEE Conference on Computer Vision and Pattern Recognition*, pages 3038–3047, 2017.
- [17] Dong-Wook Kim, Jae-Ryun Chung, Jongho Kim, Dae Yeol Lee, Se Yoon Jeong, and Seung-Won Jung. Constrained adversarial loss for generative adversarial network-based faithful image restoration. *ETRI Journal*, 41(4):415–425, 2019.
- [18] Yoonsik Kim, Jae Woong Soh, and Nam Ik Cho. Agarnet: Adaptively gated jpeg compression artifacts removal network for a wide range quality factor. *IEEE Access*, 8:20160–20170, 2020.
- [19] Hsin-Ying Lee, Hung-Yu Tseng, Jia-Bin Huang, Maneesh Singh, and Ming-Hsuan Yang. Diverse image-to-image translation via disentangled representations. In *Proceedings of the European conference on computer vision (ECCV)*, pages 35–51, 2018.
- [20] Kiryung Lee, Dong Sik Kim, and Taejeong Kim. Regression-based prediction for blocking artifact reduction in jpeg-compressed images. *IEEE Transactions on Image Processing*, 14(1):36–48, 2004.
- [21] Xianming Liu, Gene Cheung, Xiaolin Wu, and Debin Zhao. Random walk graph laplacian-based smoothness prior for soft decoding of jpeg images. *IEEE Transactions on Image Processing*, 26(2):509–524, 2016.
- [22] Xianming Liu, Xiaolin Wu, Jiantao Zhou, and Debin Zhao. Data-driven sparsity-based restoration of jpeg-compressed images in dual transform-pixel domain. In *Proceedings of the IEEE Conference on Computer Vision and Pattern Recognition*, pages 5171–5178, 2015.
- [23] D. Martin, C. Fowlkes, D. Tal, and J. Malik. A database of human segmented natural images and its application to evaluating segmentation algorithms and measuring ecological statistics. In *Proc. 8th Int'l Conf. Computer Vision*, volume 2, pages 416–423, July 2001.
- [24] Fabian Mentzer, Eirikur Agustsson, Michael Tschannen, Radu Timofte, and Luc Van Gool. Conditional probability models for deep image compression. In *Proceedings of the IEEE Conference on Computer Vision and Pattern Recognition*, pages 4394–4402, 2018.
- [25] Anish Mittal, Rajiv Soundararajan, and Alan C Bovik. Making a “completely blind” image quality analyzer. *IEEE Signal Processing Letters*, 20(3):209–212, 2012.
- [26] Takeru Miyato, Toshiki Kataoka, Masanori Koyama, and Yuichi Yoshida. Spectral normalization for generative adversarial networks. *arXiv preprint arXiv:1802.05957*, 2018.
- [27] Alexander G Ororbia, Ankur Mali, Jian Wu, Scott O’Connell, William Dreese, David Miller, and C Lee Giles. Learned neural iterative decoding for lossy image compression systems. In *2019 Data Compression Conference (DCC)*, pages 3–12. IEEE, 2019.
- [28] Tamar Rott Shaham and Tomer Michaeli. Deformation aware image compression. In *The IEEE Conference on Computer Vision and Pattern Recognition (CVPR)*, June 2018.
- [29] Olga Russakovsky, Jia Deng, Hao Su, Jonathan Krause, Sanjeev Satheesh, Sean Ma, Zhiheng Huang, Andrej Karpathy, Aditya Khosla, Michael Bernstein, et al. Imagenet large scale visual recognition challenge. *International journal of computer vision*, 115(3):211–252, 2015.
- [30] HR Sheikh. Live image quality assessment database release 2. <http://live.ece.utexas.edu/research/quality>, 2005.
- [31] Mengdi Sun, Xiaohai He, Shuhua Xiong, Chao Ren, and Xinglong Li. Reduction of jpeg compression artifacts based on dct coefficients prediction. *Neurocomputing*, 384:335–345, 2020.
- [32] Pavel Svoboda, Michal Hradis, David Barina, and Pavel Zencik. Compression artifacts removal using convolutional neural networks. *arXiv preprint arXiv:1605.00366*, 2016.
- [33] Gregory K Wallace. The jpeg still picture compression standard. *IEEE transactions on consumer electronics*, 38(1):xviii–xxxiv, 1992.
- [34] Zhangyang Wang, Ding Liu, Shiyu Chang, Qing Ling, Yingzhen Yang, and Thomas S Huang. D3: Deep dual-domain based fast restoration of jpeg-compressed images. In *Proceedings of the IEEE Conference on Computer Vision and Pattern Recognition*, pages 2764–2772, 2016.
- [35] Jaeyoung Yoo, Sang-ho Lee, and Nojun Kwak. Image restoration by estimating frequency distribution of local patches. In *The IEEE Conference on Computer Vision and Pattern Recognition (CVPR)*, June 2018.
- [36] Kai Zhang, Wangmeng Zuo, Yunjin Chen, Deyu Meng, and Lei Zhang. Beyond a gaussian denoiser: Residual learning of deep cnn for image denoising. *IEEE Transactions on Image Processing*, 26(7):3142–3155, 2017.
- [37] Xiaoshuai Zhang, Wenhan Yang, Yueyu Hu, and Jiaying Liu. Dmccn: Dual-domain multi-scale convolutional neural network for compression artifacts removal. In *2018 25th IEEE International Conference on Image Processing (ICIP)*, pages 390–394. IEEE, 2018.

- [38] Jun-Yan Zhu, Richard Zhang, Deepak Pathak, Trevor Darrell, Alexei A Efros, Oliver Wang, and Eli Shechtman. Toward multimodal image-to-image translation. In *Advances in neural information processing systems*, pages 465–476, 2017.
- [39] Simone Zini, Simone Bianco, and Raimondo Schettini. Deep residual autoencoder for blind universal jpeg restoration. *IEEE Access*, 8:63283–63294, 2020.